Environmental Science & Technology

Article

pubs.acs.org/est

CDOM Sources and Photobleaching Control Quantum Yields for Oceanic DMS Photolysis

Martí Galí,[*,†] David J. Kieber,[‡] Cristina Romera-Castillo,[§,∥] Joanna D. Kinsey,[‡,⊥] Emmanuel Devred,[†,#] Gonzalo L. Pérez,[▽] George R. Westby,[‡] Cèlia Marrasé,[¶] Marcel Babin,[†] Maurice Levasseur,[†] Carlos M. Duarte,[○] Susana Agustí,[○] and Rafel Simó[¶]

[†]Takuvik Joint International Laboratory (Université Laval – CNRS), Biology Department, Université Laval, 1045 Avenue de la Médecine, G1 V 0A6 Québec, Quebec, Canada

[‡]Department of Chemistry, College of Environmental Science and Forestry, State University of New York, 1 Forestry Drive, Syracuse, New York 13210, United States

[§]Rosenstiel School of Marine and Atmospheric Science, RSMAS/OCE, University of Miami, Miami, Florida 33149, United States

[∥]Department of Limnology and Bio-Oceanography, Center of Ecology, University of Vienna, 1090 Vienna, Austria

[⊥]Department of Marine, Earth and Atmospheric Sciences, North Carolina State University, 2800 Faucette Drive, Raleigh, North Carolina 27695, United States

[#]Fisheries and Oceans Canada, Bedford Institute of Oceanography, Dartmouth, NS B2Y 4A2, Canada

[▽]Instituto INIBIOMA (CRUB Comahue, CONICET), Quintral 1250, 8400 S.C. de Bariloche, Rio Negro, Argentina

[¶]Department of Marine Biology and Oceanography, Institut de Ciències del Mar (CSIC), Passeig Marítim de la Barceloneta 37-49, 08003 Barcelona, Catalonia Spain

[○]King Abdullah University of Science and Technology (KAUST), Red Sea Research Center (RSRC), Thuwal, 23955-6900, Saudi Arabia

Supporting Information

ABSTRACT: Photolysis is a major removal pathway for the biogenic gas dimethylsulfide (DMS) in the surface ocean. Here we tested the hypothesis that apparent quantum yields (AQY) for DMS photolysis varied according to the quantity and quality of its photosensitizers, chiefly chromophoric dissolved organic matter (CDOM) and nitrate. AQY compiled from the literature and unpublished studies ranged across 3 orders of magnitude at the 330 nm reference wavelength. The smallest AQY(330) were observed in coastal waters receiving major riverine inputs of terrestrial CDOM (0.06–0.5 m^3 (mol quanta)$^{-1}$). In open-ocean waters, AQY(330) generally ranged between 1 and 10 m^3 (mol quanta)$^{-1}$. The largest AQY(330), up to 34 m^3 (mol quanta)$^{-1}$), were seen in the Southern Ocean potentially associated with upwelling. Despite the large AQY variability, daily photolysis rate constants at the sea surface spanned a smaller range (0.04–3.7 d^{-1}), mainly because of the inverse relationship between CDOM absorption and AQY. Comparison of AQY(330) with CDOM spectral signatures suggests there is an interplay between CDOM origin (terrestrial versus marine) and photobleaching that controls variations in AQYs, with a secondary role for nitrate. Our results can be used for regional or large-scale assessment of DMS photolysis rates in future studies.

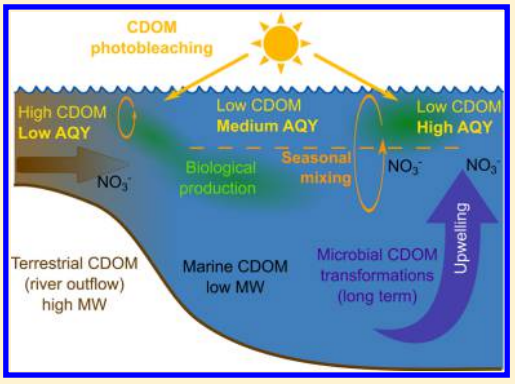

1. INTRODUCTION

Dimethylsulfide (DMS) is primarily produced in the sunlit layer of the ocean from microbial transformations of dimethylsulfoniopropionate (DMSP),[1,2] a multifunctional osmolyte synthesized by phytoplankton, macroalgae, and corals.[3] The sea-air flux of DMS, estimated at 20–28 Tg S y^{-1} (ref[4,5]), is large compared to many other marine organic volatiles.[6,7] Ocean-emitted DMS can affect climate through its effects on aerosol and cloud formation,[8−10] and DMS plays an important ecological role as an infochemical.[11,12] However, the sea–air DMS flux represents only a small fraction (generally 5—15%) of the DMS produced in the upper mixed layer (UML) of the ocean.[13] The remainder is removed from the water column through biological[14] and photochemical[15,16] processes. In a shallow upper mixed layer (UML) and under

Received: August 23, 2016
Revised: November 11, 2016
Accepted: November 14, 2016
Published: November 14, 2016

DOI: 10.1021/acs.est.6b04278
Environ. Sci. Technol. XXXX, XXX, XXX−XXX

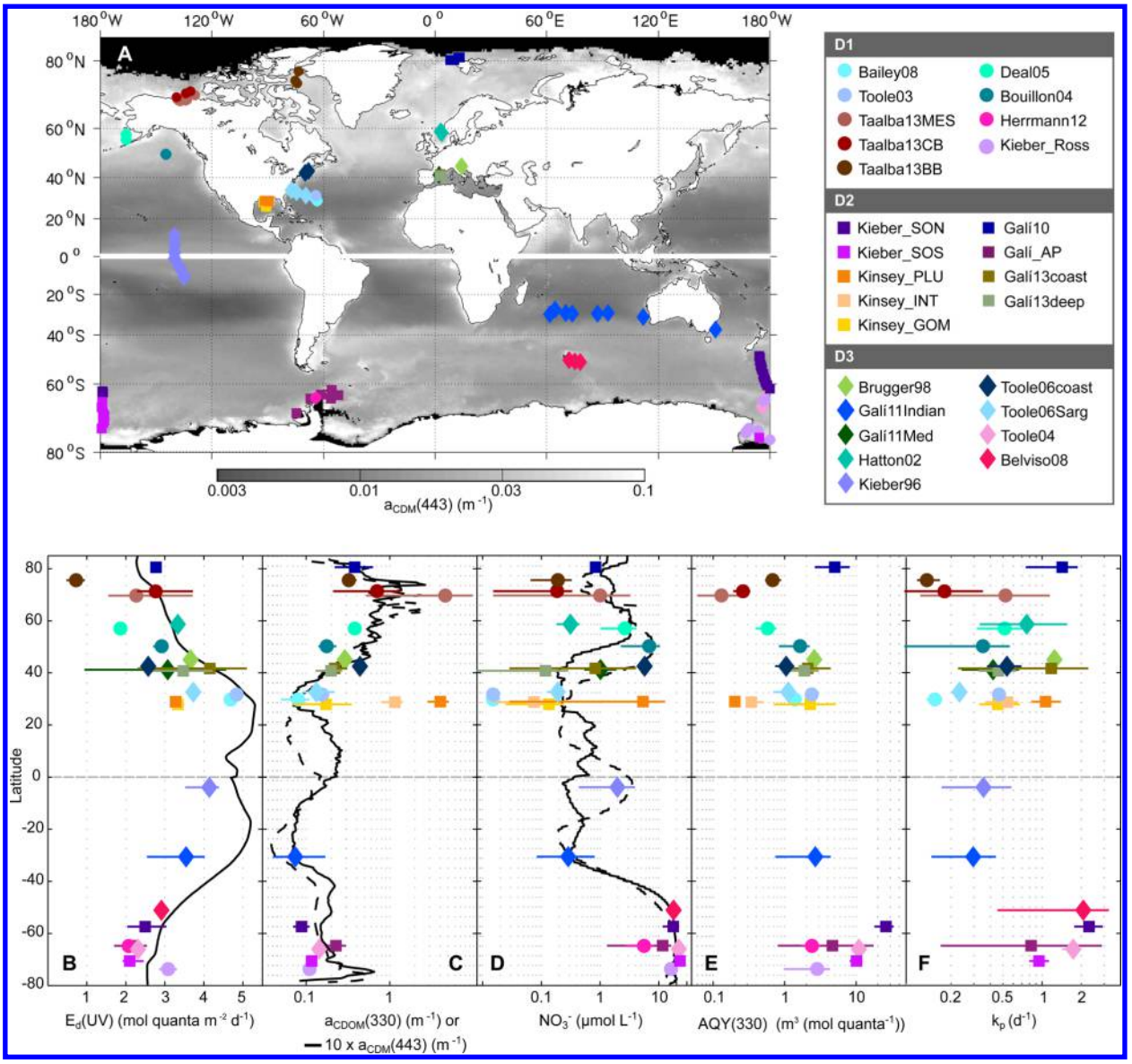

Figure 1. (A) Sampling locations overlaid on a global map of satellite-retrieved $a_{CDM}(443)$ (CDM stands for colored detrital and dissolved materials, a proxy for CDOM;[27] SeaWiFS sensor 1998−2010 climatology). Panels B through F display the latitudinal patterns of photolysis variables at the sea surface in each study (median and range). Black lines in B−D represent zonal averages of climatological data from April through September (northern hemisphere) or October through March (southern hemisphere). In C and D, solid lines represent the Atlantic and Indian basins and dashed lines the Pacific basin. (B) Climatological daily UV irradiance (290 to 400 nm). (C) In situ $a_{CDOM}(330)$ and satellite $a_{CDM}(443)$ climatology (scaled by 10×); (D) Nitrate concentration in situ and in a global climatology;[34] (E) apparent quantum yields for DMS photolysis at 330 nm (AQY(330)); (F) daily DMS photolysis rate constants just below the sea surface (k_p). Symbols of different colors represent published and unpublished studies identified in the legend. Different symbols distinguish studies classified into subsets D1, D2, and D3 (see text). The same color/symbol coding is followed throughout the paper.

high-irradiance conditions typical of summer, photolysis can become the main removal mechanism for DMS,[13,17−19] controlling its sea-surface concentration and flux into the atmosphere.[13]

DMS does not absorb photons at the solar wavelengths that reach the Earth's surface. Rather, it is oxidized by reactive species generated upon light absorption by optically active substances in seawater known as photosensitizers.[15] It is generally assumed that chromophoric dissolved organic matter (CDOM) and nitrate[20] are the main DMS photosensitizers in seawater. Although several studies have reported on the kinetics and the spectral dependence of DMS photolysis in different marine and estuarine environments, the factors that control the observed variability in DMS photolysis rates, and the relative importance of CDOM and nitrate as photosensitizers, remain controversial.[21,22] Even less is known about the molecular-scale mechanisms of DMS photolysis, the specific oxidants involved (e.g., the hydroxyl radical or other radical species[20,23]) and their temperature dependence.[24] This limits our ability to model DMS photolysis across contrasting marine environments and to predict its future trends under global-change scenarios.

DMS photolysis follows pseudo-first order kinetics[16,23] at ambient seawater DMS concentrations.[16] Thus, instantaneous photolysis rates (d[DMS]/dt) can be calculated as the product of the pseudo first-order rate constant (k_p) and DMS concentration:

DOI: 10.1021/acs.est.6b04278
Environ. Sci. Technol. XXXX, XXX, XXX−XXX

Table 1. Summary Statistics[a] for the Compiled AQY for DMS Photolysis at 330 nm, (AQY(330), m^3 (mol quanta)$^{-1}$), and the Daily Pseudo-First Order Rate Constants at the Sea Surface (k_p, d^{-1}), for Different Biogeochemical Domains and Open Ocean Sub-Domains (Latitude Bands)

biogeochemical domain		AQY(330)				k_p (d^{-1})			
		median	Q25%	Q75%	*n*	median	Q25%	Q75%	*n*
river-influenced coasts		0.13[a]	0.08	0.23	19	0.58[a]	0.43	0.88	19
other coastal/shelf areas		2.30[bc]	1.45	3.13	15	0.68[ab]	0.38	1.57	19
	north of 65°N	0.53[b]	0.25	3.0	13	0.28[abc]	0.11	1.05	13
	65°N to 35°N	1.66[b]	0.91	2.19	16	0.42[ac]	0.34	0.58	20
open ocean	35°N to 35°S	1.80[b]	1.33	2.65	23	0.35[c]	0.23	0.43	33
	35°S to 65°S	22.0[d]	18.0	30.7	22	2.17[d]	1.78	2.53	26
	South of 65°S	6.40[c]	3.29	10.5	27	0.98[bd]	0.85	1.41	15

[a]Differences between biogeochemical domain and subdomain medians are shown with superscript letters. Sample groups that do not share the same superscript letters are significantly different with $\alpha = 0.05$. Pairwise differences were tested with the Mann−Whitney U-test (Bonferroni-adjusted *p* values) after testing for significant differences among groups (Kruskal−Wallis test; $p < 10^{-9}$ for both AQY(330) and k_p).

$$d[DMS]/dt = k_p[DMS] \quad (1)$$

In turn, k_p can be modeled as the product of three spectral variables integrated across the relevant wavelength range (Supporting Information (SI) Figure S1):

$$k_p = \int E_d(\lambda) a_{CDOM}(\lambda) AQY(\lambda) d\lambda \quad (2)$$

where $E_d(\lambda)$ is the downwelling irradiance (mol quanta m^{-2} s^{-1}), $a_{CDOM}(\lambda)$ is the CDOM absorption coefficient (m^{-1}), and $AQY(\lambda)$ is the apparent quantum yield for DMS photolysis [m^3 (mol quanta)$^{-1}$].

An AQY is used here instead of a true quantum yield to define the efficiency for DMS photolysis because the precursors giving rise to DMS photolysis in seawater are not known and therefore the absorption term includes all components of CDOM, including contributions of light-absorbing substances (chromophores) that do not participate in DMS photolysis. Thus, wavelength-dependent AQY are minimum estimates of the true wavelength-dependent quantum yields. In general, AQYs decrease exponentially with increasing wavelength[21,24−26] and become insignificant at wavelengths longer than 400 nm, as is the case for DMS photolysis. The photolysis of DMS is driven by ultraviolet (UV) radiation between 300 and 400 nm in seawater, with a peak near 330 nm.[21,24−26]

Generally, CDOM is the main absorber of UV radiation and thus controls UV penetration in oceanic waters.[27] CDOM absorption coefficients typically decrease sharply from river-influenced coastal waters to offshore waters, reflecting the balance between photobleaching of terrestrially derived CDOM, autochthonous CDOM production[28,29] and mixing between the oceanic and coastal end-members.[27] Owing to its characteristic optical signature, CDOM can be monitored using ocean color remote sensing,[27] enabling large-scale photochemistry assessments. Satellite-based estimates of photochemical rates have been made for dissolved organic carbon (DOC) photomineralization[30] and for carbon monoxide photoproduction[31] in seawater. Yet, to our knowledge this approach has not been applied to DMS photolysis, likely because a synthesis study of DMS photolysis AQYs is missing. Here we analyze the variability in DMS photolysis rate constants and AQYs in a comprehensive global data set, gaining insights into the environmental factors affecting photolysis. This should improve our ability to remotely sense and model DMS photolysis in surface waters globally.

2. MATERIALS AND METHODS

2.1. Database. We assembled a global database of DMS photolysis measurements in the upper mixed layer of the ocean, including both published and previously unpublished data (Figure 1 and SI Table S1). Individual studies were labeled with the name of the lead author followed by the publication year, or with the name of the authors followed by the study area in the case of unpublished studies. Some studies were divided into two or three regions according to the authors' criteria. We did not apply any correction to the data reported in the original papers, and the reader is referred to Table S2 for methodological details of each study. The data were assigned to three different subsets (D1-D3) according to the type of measurements performed and the increasing uncertainty of AQY estimation:

D1 ($n = 50$): Studies specifically designed to measure AQY (see section 2.4).

D2 ($n = 78$): Studies where k_p was determined in at least one spectral treatment along with a_{CDOM} spectra and spectral UV downwelling irradiances (E_d). This allowed AQY to be determined at the reference wavelength (330 nm) using a spectral optimization method after making a few simplifying assumptions (see section 2.5).

D3 ($n = 18$): k_p was determined, but a_{CDOM} and/or UV irradiances did not have sufficient spectral resolution to determine AQY(330) with the methodology used for the D2 subset. Instead, AQY(330) for this data set were estimated from a fitted equation based on data from the D1 and D2 subsets (see section 2.6).

Samples were further classified into three biogeochemical domains: *river-influenced coastal waters* that include the Mackenzie Estuary and Shelf ("Taalba13MES" subset), plus the Mississippi plume ("Kinsey_PLU") and its transitional waters toward the Gulf of Mexico at a distance less than 50 km from the coast ("Kinsey_INT"); *other coastal/shelf areas* that include samples collected less than 50 km from the coast over a water column shallower than 200 m and excluding river-influenced waters; and the *open ocean* that includes the remaining samples.

When available, ancillary variables were reported including temperature in situ and during the incubation, salinity, nitrate concentration (nitrate + nitrite in some studies), chlorophyll *a*, and dissolved organic carbon concentration (DOC). Missing temperature, salinity and nitrate data were filled with climatological data from the World Ocean Atlas[32−34] (only for open-ocean samples), and missing bottom depths were

DOI: 10.1021/acs.est.6b04278
Environ. Sci. Technol. XXXX, XXX, XXX−XXX

obtained from the General Bathymetric Chart of the Oceans (www.gebco.net/). Available CDOM spectra were used to compute (i) the spectral slope ratio S_R, defined as S_{275_295}/S_{350_400} where S is the spectral slope of $\ln(a_{CDOM})$ for the spectral intervals 275—295 nm and 350—400 nm;[35] (ii) the absorbance ratio between 254 and 365 nm, $a_{CDOM}(254)/a_{CDOM}(365)$;[36] and (iii) the specific ultraviolet absorption (often referred to as SUVA)[37] defined as $a_{CDOM}(254)$/DOC. S_R and $a_{CDOM}(254)/a_{CDOM}(365)$ are proxies for the mean CDOM molecular weight and degree of photobleaching, whereas $a_{CDOM}(254)$/DOC is a proxy for aromaticity.

Our analysis includes only the results from filtered seawater incubations, precluding any assessment of particle-associated DMS photolysis. Measurement of particle-associated DMS photolysis is challenging[20] due to concurrent DMS photoproduction by marine particles,[18,38] and might be important in detritus- and sediment-laden coastal waters.[20]

All statistical analyses were done using Matlab 2013b, except for the statistics shown in Table 1 that were calculated using R 3.2.0[39] (multcompView package[40]). Significance thresholds and reported confidence intervals correspond to $\alpha = 0.05$. Throughout the text, r refers to Pearson's linear correlation coefficient and r_S to Spearman's rank correlation coefficient.

2.2. Radiative Transfer Model. The downwelling spectral irradiance just below the sea surface, $E_{d,0^-}(\lambda)$, was computed using the Santa Barbara DISORT Atmospheric Radiative Transfer (SBDART)[41] model as implemented by Bélanger et al. (ref 42). In this configuration, SBDART outputs the spectral irradiance (μmol quanta m^{-2} s^{-1}) at a given location every 3 h at a spectral resolution of 5 nm between 290 and 700 nm using climatological satellite-observed atmospheric properties at each location and date. Further details on SBDART implementation are given in SI section 1.

2.3. k_p Determination and Scaling to Daily Irradiance. The pseudo-first order rate constant can be determined by evaluating DMS loss over time under controlled irradiance using the integrated form of eq 1:

$$k_{p,OBS} = \ln([DMS]_0/[DMS])/t \quad (3)$$

where $k_{p,OBS}$ is the observed photolysis rate constant, $[DMS]_o$ is the initial DMS concentration and [DMS] is the concentration at irradiation time t. In the compiled studies, $k_{p,OBS}$ was expressed in several different units. To allow for a comparison, all the $k_{p,OBS}$ were normalized to the daily climatological irradiance at their corresponding sampling location using the equation:

$$k_p = k_{p,OBS}E_{d,day}/E_{d,INCUB} \quad (4)$$

where $E_{d,INCUB}$ is the reported incubation irradiance and $E_{d,day}$ is the daily climatological irradiance calculated with SBDART, integrated within the same radiation band that was reported in each study (see SI section 2). Note that normalization to the particular band reported in each study would have been nearly impossible without the use of a spectrally resolved radiative transfer model. When $k_{p,OBS}$ was reported in photon dose^{-1} units, k_p was converted to d^{-1} units assuming reciprocity.[43] Henceforth, k_p in our study is expressed in d^{-1} and represents the pseudo-first order photolysis rate constant just below the sea surface for a given location and date and the corresponding 24 h climatological irradiance.

2.4. AQY(λ) Determination in the D1 Subset. Studies belonging to the D1 subset were designed to determine AQY(λ) using a *monochromatic*[24,25] or *polychromatic*[21,26] approach, as described elsewhere. Results obtained from both approaches indicate that the AQY spectrum for DMS photolysis can be modeled using a decreasing exponential function:

$$AQY(\lambda) = AQY_{ref}\exp[S_{AQY}(\lambda - \lambda_{ref})] \quad (5)$$

where AQY_{ref} is the AQY at the reference wavelength, λ_{ref}, and S_{AQY} is the AQY spectral slope. Here we set the reference wavelength at 330 nm, corresponding to the peak in the photolysis response,[21,24−26] and converted AQY(λ) reported at different wavelengths to AQY(330) using eq 5 when needed. The unit for the DMS AQY is m^3 (mol quanta)$^{-1}$. This is equivalent to 10^{-6} mol DMS photolyzed per mol quanta normalized to 1 nmol L^{-1} DMS, as used in other studies.[24]

2.5. AQY(330) Determination in the D2 Subset. Studies designated as D2 were not designed to determine AQY(λ). Yet, since a_{CDOM} and irradiance spectra between 300 and 400 nm were accurately known, we were able to use a nonlinear optimization method to determine the AQY spectrum that satisfied the observed k_p, according to eq 2 and 5 (see SI for methodological details). This approach is similar to that employed for polychromatic D1 incubations except that, when the experimental k_p was determined under a single spectral treatment, it required making assumptions regarding the value of S_{AQY}. That is, since S_{AQY} could not be estimated through optimization, an S_{AQY} value was chosen a priori to estimate AQY(330) through optimization. The sensitivity of optimized AQY(330) to the chosen S_{AQY} was estimated by calculating AQY(330) for 13 S_{AQY} values ranging between 0.0200 and 0.0700 nm^{-1} (see section 3.2). This test showed that, on average, estimated AQY(330) varied by ±36% (relative standard deviation about the mean) between the smallest and the largest S_{AQY} values tested. We took the mean of the 13 AQY(330) and assumed that this coefficient of variation represented the maximum error associated with AQY(330) in the D2 subset. The uncertainty was also computed over a narrower spectral-slope range, between 0.034 and 0.058 nm^{-1}, which encompassed the open-ocean AQY spectra. This yielded a correspondingly smaller uncertainty (<±10%) in AQY(330).

Occasionally, k_p was determined under two to four spectral treatments in samples classified in the D2 subset.[38] This allowed for the determination of both AQY(330) and S_{AQY} following the same polychromatic modeling approach that was used for the D1 subset, but with larger uncertainty due to the smaller number of spectral treatments applied.

2.6. AQY(330) Determination in the D3 Subset. The photolysis of DMS just below the sea surface generally peaks around 330 nm[21,24−26] (SI Figure S1), suggesting that k_p should be roughly proportional to the product $E_d(330)$ $a_{CDOM}(330)$ AQY(330). Here we took advantage of this spectral response to derive an empirical method to estimate AQY(330). In the first step, a standardized daily photolysis rate constant, k^*_p, was calculated by scaling k_p to an arbitrary standard daily irradiance ($E_{d,daySTA}$). For the D1 subset, k^*_p was calculated through forward application of eq 2 when the in situ $a_{CDOM}(\lambda)$ was available. For D2 and D3, it was estimated as

$$k^*_p = k_pE_{d,daySTA}/E_{d,dayINCUB} \quad (6)$$

where $E_{d,daySTA}$ is the output of SBDART at 45°N and 30°W for June 21 (summer solstice). For D2 and D3, eq 6 was applied using a broadband irradiance value obtained by integrating the

DOI: 10.1021/acs.est.6b04278
Environ. Sci. Technol. XXXX, XXX, XXX−XXX

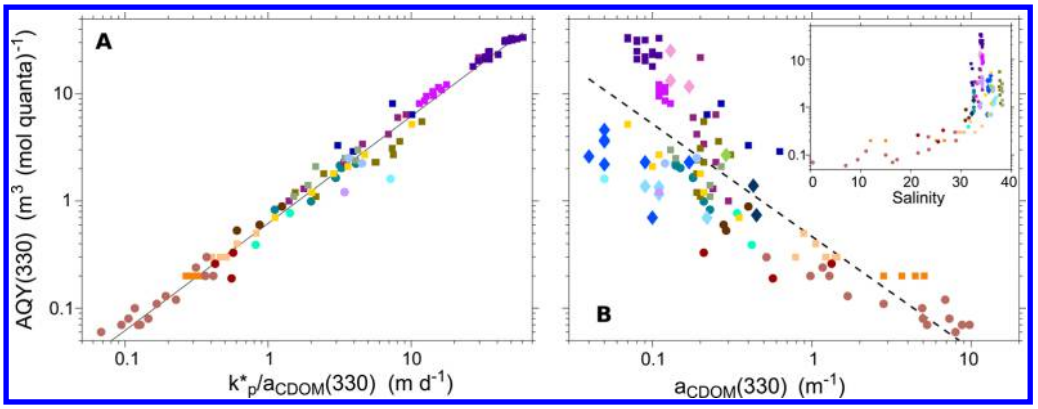

Figure 2. (A) Relationship between AQY(330) and the quotient $k^*_p/a_{CDOM}(330)$ (eq 7). k^*_p is the DMS photolysis rate constant just below the sea surface scaled to a fixed standard irradiance spectrum. (B) Relationship between AQY(330) and $a_{CDOM}(330)$. Inset: Relationship between AQY(330) and salinity. In B, AQY(330) marked with diamonds (subset D3) were estimated from the linear fit shown in Figure 2A (eq 7), and were not used to derive the regression depicted by the dashed line (eq 8). See Figure 1 for a legend to the symbols and colors corresponding to different studies.

$E_{d,daySTA}$ spectrum across the same radiation band that was monitored during each incubation ($E_{d,dayINCUB}$), as done in section 2.3.

In the second step, k^*_p was used to plot AQY(330) from the D1 and D2 subsets against $k^*_p/a_{CDOM}(330)$ to obtain the following regression eq (Figure 2A):

$$\log_{10} AQY(330) = (-0.21 \pm 0.01) + (1.00 \pm 0.01) \log_{10}[k^*_p/a_{CDOM}(330)] \quad (7)$$

with $r^2 = 0.99$, $n = 111$ (type II major axis regression). The highly significant relationship confirmed that the broadband photolysis of DMS in seawater exposed to sea-surface solar radiation can be approximated by the peak response wavelength at 330 nm. Furthermore, this procedure allowed us to include in our analysis AQY(330) data from the D3 subset (or, more generally, any samples where only $a_{CDOM}(330)$, k_p and the broadband irradiance were known).

3. RESULTS AND DISCUSSION

3.1. k_p and AQY(330) variability. Our data set covers a wide environmental range spanning the Arctic through temperate and tropical oceans to the Antarctic Seas, and from estuarine and coastal areas to the open ocean (Figure 1). Since most measurements were obtained between the spring and fall equinoxes, the daily UV irradiance typically varied within a relatively narrow range (Figure 1B). By contrast, a_{CDOM}, nitrate and AQY(330) varied by 2−3 orders of magnitude both across latitudes and from oceanic to coastal waters (Figure 1C−E), suggesting that their role in controlling k_p variability was more important than that of irradiance. Since the patterns displayed by a_{CDOM} and nitrate have been described elsewhere, below we examine the variability of the daily DMS photolysis rate constants at the sea surface (k_p) and the corresponding AQY(330).

In the ensemble of studies, k_p varied between 0.044 and 3.66 d^{-1}, with a median of 0.55 d^{-1}, and displayed regular oceanographic patterns (Table 1, Figure 1F). Typically, k_p ranged between 0.2 and 0.6 d^{-1} in low-latitude (35°S to 35°N) open ocean environments[16,24,44,45] and in temperate[46] to subpolar[21,25,47] northern hemisphere oceans, with slightly lower k_p at low latitudes. A larger scatter was observed in northern polar seas, with an overall median of 0.28 d^{-1} but with higher k_p in the Greenland Sea[19] compared to the Beaufort Sea and the northern Baffin Bay.[26] Higher k_p of ca. 1 d^{-1} were observed in waters nearby the Antarctic Peninsula and in the Ross Sea; yet, the highest k_p values (median 2.2 d^{-1}) were consistently observed in the Southern Ocean[22,48] particularly at latitudes between 50° and 70°S in the Indian and Pacific sectors.

In the open ocean, the 50% central values (interquartile range) of AQY(330) were between 1.3 and 10.5 m^3 (mol quanta)$^{-1}$, with a median of 3.1 m^3 (mol quanta)$^{-1}$. In tropical and subtropical oceans, as well as in northern temperate to subpolar seas, the median AQY(330) was 1.7 m^3 (mol quanta)$^{-1}$. A larger scatter was observed at latitudes above 65°N, with values up to 8 m^3 (mol quanta)$^{-1}$ in the Greenland Sea but less than 1 m^3 (mol quanta)$^{-1}$ in the northern Baffin Bay. Moderate to high values were observed south of 65°S, with a median of 6.4 m^3 (mol quanta)$^{-1}$. As with k_p, the highest AQY(330) were seen in Sub-Antarctic waters with a maximum of 34 m^3 (mol quanta)$^{-1}$. Previously, the highest AQY(330) reported in the literature was 2.5 m^3 (mol quanta)$^{-1}$ in the Sargasso Sea.[24] Therefore, our study extends the upper range of DMS photolysis AQY by an order of magnitude, and indicates that AQY(330) between 3 and 34 m^3 (mol quanta)$^{-1}$ are not exceptional. The maximum AQY(330) occurred within a narrow range in salinity and temperature characteristic of the Antarctic Polar Front,[49] suggesting a link with upwelling of deep, potentially old[50] water masses (SI Figure S2).

Coastal waters influenced by the Mackenzie[26] and the Mississippi River outflows differed from the general patterns in k_p and AQY(330) seen in the open ocean, adding another dimension (inshore-offshore) to the latitudinal gradients. A closer examination of these coastal transects showed that k_p increased by four- to 10-fold toward the mouth of these major rivers compared to nearby oceanic waters (e.g., compare "Kinsey_PLU" to "Kinsey_INT" and "Kinsey_GOM", and "Taalba13MES" to "Taalba13CB" in Figure 1). This trend corresponded to a 40−70-fold increase in $a_{CDOM}(330)$ and a ca. 5-fold decrease in AQY(330) with decreasing salinity, such that AQY(330) was usually less than 0.2 m^3 (mol quanta)$^{-1}$ close to river mouths (Figure 2B inset). Pooling together these two river-influenced coastal data sets, the linear correlation coefficient between AQY(330) and salinity for salinities less than 31 was $r = 0.78$ ($p = 3 \times 10^{-6}$, $n = 25$). For comparison,

DOI: 10.1021/acs.est.6b04278
Environ. Sci. Technol. XXXX, XXX, XXX−XXX

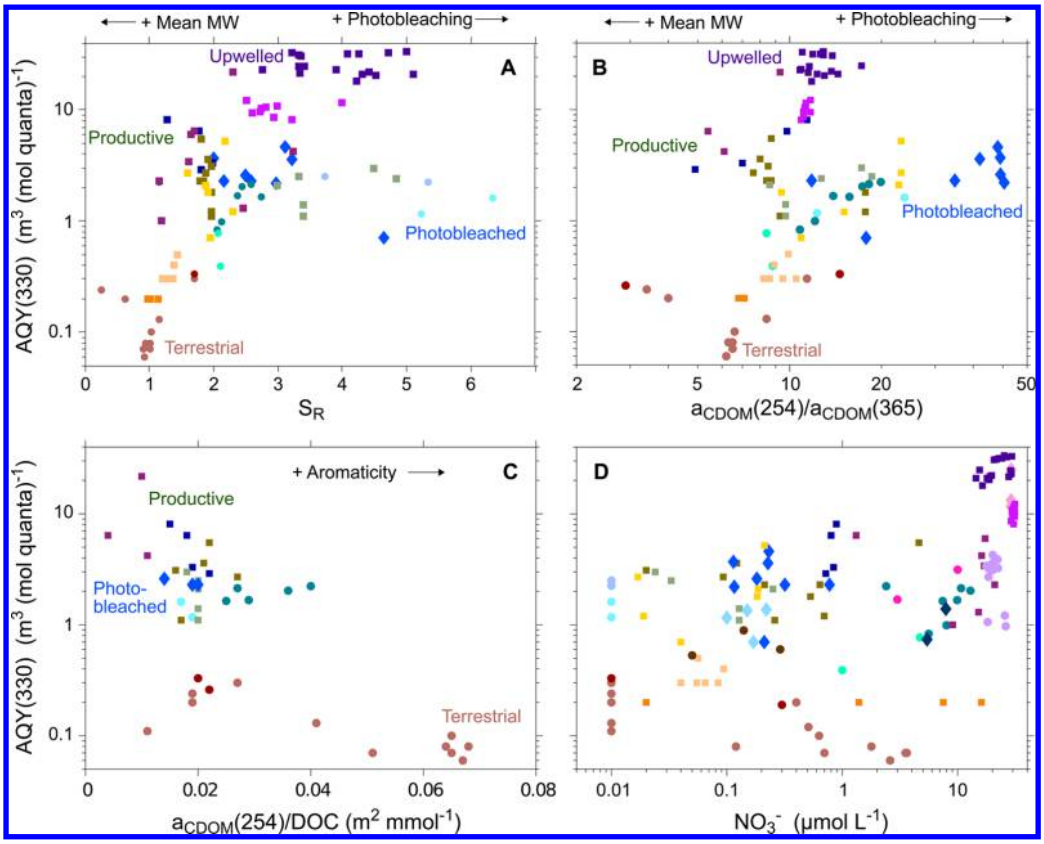

Figure 3. Relationship between AQY(330) and (A) the CDOM spectral slope ratio S_R; (B) the CDOM absorbance ratio at 254 and 365 nm; (C) the $a_{CDOM}(254)$/DOC ratio (specific UV absorption); and (D) the nitrate concentration. Diamonds denote AQY(330) estimated from eq 7. In A–C, different end members were tentatively identified as terrestrial, photobleached, productive, and upwelled surface waters (see sections 3.1, 3.2, and 3.6). MW: CDOM molecular weight. See Figure 1 for the legend to the symbols and colors corresponding to different studies.

the correlation between $a_{CDOM}(330)$ and salinity was $r = -0.95$ for the same pooled data sets. Because of the opposite changes in $a_{CDOM}(330)$ and AQY(330), k_p in river-influenced waters were not significantly different, overall, from those in other coastal areas (Table 1). In samples from coastal and continental shelf areas with limited or no riverine influence, such as those from the coastal NW Mediterranean,[38,45,51] NW Atlantic[18] and Antarctica,[52] k_p and AQY(330) were similar or slightly higher than those in temperate to subpolar oceanic waters (excluding the Sub-Antarctic region).

3.2. AQY and a_{CDOM} Magnitude and Spectral Shape. When the full range of AQY(330) and $a_{CDOM}(330)$ was examined (Figure 2B), a highly significant inverse relationship was found between $\log_{10}$AQY(330) and $\log_{10}a_{CDOM}(330)$, according to the regression equation:

$$\log_{10} \mathrm{AQY}(330) = (-0.32 \pm 0.11) - (1.08 \pm 0.13) \log_{10} a_{CDOM}(330) \quad (8)$$

with $r^2 = 0.70$, $p < 10^{-16}$, $n = 111$. The D3 subset was not included in the regression, since it was derived from another regression involving $a_{CDOM}(330)$. At $a_{CDOM}(330)$ less than 0.4 m^{-1}, characteristic of oceanic waters, the AQY(330) vs $a_{CDOM}(330)$ relationship diverged into two distinct trends, roughly defined by high- and low-latitude samples. This divergence was more marked at low $a_{CDOM}(330)$, with AQY(330) ranging between 1 and 34 m^3 (mol quanta)$^{-1}$ at $a_{CDOM}(330)$ of 0.1 m^{-1}.

AQY(330) from different study areas were grouped according to the value of spectroscopic indicators of CDOM origin, molecular weight and photobleaching (Figure 3). AQY(330) generally increased with S_R and the $a_{CDOM}(254)$/$a_{CDOM}(365)$ ratio and decreased with the $a_{CDOM}(254)$/DOC ratio. Low AQY(330) characteristic of river outflow areas coincided with the lowest spectral slope ratios ($S_R < 2$, Figure 3A), low to intermediate values of the $a_{CDOM}(254)$/$a_{CDOM}(365)$ ratio (3–15, Figure 3B) and intermediate to high $a_{CDOM}(254)$/DOC ratios (generally 0.02–0.07 m^2 $mmol^{-1}$, Figure 3C). Furthermore, AQY(330) in river-influenced samples showed a monotonic increase with S_R ($r_S = 0.75$, $p = 10^{-4}$, $n = 21$) and the $a_{CDOM}(254)$/ $a_{CDOM}(365)$ ratio ($r_S = 0.74$, $p = 7 \times 10^{-5}$), and a decrease with $a_{CDOM}(254)$/DOC ($r_S = -0.72$, $p = 0.01$). Overall, this suggests that the offshore increase in AQY(330) is related to photobleaching of terrestrial CDOM, accompanied by a decrease in the mean CDOM molecular weight[35] and CDOM aromaticity.[37]

In oceanic waters, the relationship between AQY(330) and S_R branched at $S_R > 2$, setting apart high-AQY Sub-Antarctic waters from other oceanic regions (Figure 3A). Samples from diverse subtropical to subpolar seas clustered around an S_R of 2, whereas samples with S_R between 3.5 and 6.3 and AQY(330) smaller than 4 m^3 (mol quanta)$^{-1}$ originated mainly from the open Mediterranean Sea and the subtropical gyres, with maximal S_R in the Sargasso Sea (July-August). Comparison between AQY(330) and the $a_{CDOM}(254)/a_{CDOM}(365)$ ratio revealed a similar branching pattern, with separation into two

DOI: 10.1021/acs.est.6b04278
Environ. Sci. Technol. XXXX, XXX, XXX–XXX

groups at $a_{CDOM}(254)/a_{CDOM}(365)$ of ca. 10. The grouping of samples was, however, slightly different from that produced by S_R. In this case, the samples from the Indian Ocean subtropical gyre in late austral summer showed the highest $a_{CDOM}(254)/a_{CDOM}(365)$ ratio with values above 30. High S_R and $a_{CDOM}(254)/a_{CDOM}(365)$ have both been interpreted as the signature of intense CDOM photobleaching at the sea surface, which is overall consistent with the observed trends. The high S_R (with a maximum of 5 at 60°S) seen in high-AQY Sub-Antarctic samples in the austral spring is more intriguing, and perhaps related to CDOM transformations other than photobleaching.[53]

Despite the general positive covariation between AQY(330) and either S_R or $a_{CDOM}(254)/a_{CDOM}(365)$, both indices showed a local minimum in samples from the Greenland Sea and the Antarctic Peninsula with AQY(330) between 1 and 10 m^3 (mol quanta)$^{-1}$. This pattern might reflect the effect of higher local biological productivity on the CDOM pool, since these samples exhibited a higher median chlorophyll concentration (0.69 $\mu g\ L^{-1}$) than the other oceanic samples (ca. 0.20 $\mu g\ L^{-1}$). Yet, this interpretation remains speculative.

The inverse relationship between AQY and a_{CDOM} at the 330 nm reference wavelength extended across the spectral domain. The median AQY spectral slope (S_{AQY}) in the Mackenzie estuary and shelf (0.0275 nm^{-1}, $n = 14$) was significantly smaller ($p = 0.0002$, Kruskal–Wallis test) than in oceanic samples (0.0462 nm^{-1}, $n = 36$). In fact, $\log_{10}$AQY(330) and S_{AQY} displayed a significant positive linear correlation in the D1 subset studies ($r = 0.54$, $p = 2 \times 10^{-4}$, $n = 47$; SI Figure S3). This suggests that the AQY spectrum becomes steeper and thus shortwave-shifted as it increases in magnitude.

As described in Section 2.5, we estimated S_{AQY} in some D2 samples that could then be compared to D1 samples, and a good agreement between both subsets was found (SI section 3). Interestingly, S_{AQY} in samples from the Sub-Antarctic and Antarctic Peninsula region was significantly higher than in the other oceanic samples ($p = 2 \times 10^{-5}$, Kruskal–Wallis test; pooled D1 and D2 subsets). The median of Sub-Antarctic and Antarctic Peninsula samples was 0.0535 nm^{-1} (n = 23), compared to 0.0389 nm^{-1} in the rest of oceanic samples ($n = 29$). These results indicate that high AQY and steep AQY spectral slopes are characteristic of Antarctic waters and set them apart from other oceanic regions including Arctic waters.

3.3. AQY and Nitrate. The role of nitrate as a DMS photosensitizer was previously examined in two studies. In the Northeast Pacific, AQY(330) increased with nitrate concentration at a rate of 0.15 m^3 (mol quanta)$^{-1}$ μM^{-1} ($n = 7$; "Bouillon2004" data set).[21] In the Southern Ocean, k_p increased linearly with added nitrate which corresponded to a slope between 0.17 and 0.19 m^3 (mol quanta)$^{-1}$ μM^{-1} ("Toole2004" data set,[22] SI section 4). In our data set, we further assessed the role of nitrate by regressing the residuals left after fitting AQY(330) to $a_{CDOM}(330)$ (eq 8) against nitrate concentration (SI Figure S4A). This gave a regression slope of 0.17 ± 0.04 m^3 (mol quanta)$^{-1}$ μM^{-1} ($r^2 = 0.41$, $p < 10^{-12}$, $n = 111$), similar to the nitrate dependence calculated from the two previous regional studies. The slope was not significantly different if river-influenced samples were excluded.

Figure 3D displays the relationship between AQY(330) and nitrate. Despite the visual scatter, a highly significant correlation existed between the two variables ($r = 0.55$, $p < 10^{-10}$; $r_S = 0.64$, $p < 10^{-16}$; log-transformed variables). However, as discussed in the previous paragraph, assuming that AQY(330) increases at a rate of 0.17 m^3 (mol quanta)$^{-1}$ μM^{-1}, AQY(330) would be expected to increase by only 5 m^3 (mol quanta)$^{-1}$ for a 30 μM nitrate increase, such as that found between subtropical gyres and Southern Ocean surface waters, compared to the observed increase in AQY(330) of nearly 20 m^3 (mol quanta)$^{-1}$ (Table 1).

Further insights can be gained by examining seasonal AQY(330) variations (SI Figure S5). In the coastal Northwest Mediterranean,[38] a maximal AQY(330) of 5.5 ± 0.5 m^3 (mol quanta)$^{-1}$ was observed in late winter, with nitrate of 4.6 μM, compared to a mean ± std AQY(330) of 1.8 ± 0.7 in spring and summer ($n = 8$), with nitrate of 0.32 ± 0.26 μM. In this case, nitrate would explain a change in AQY(330) of 0.73 m^3 (mol quanta)$^{-1}$, 23% of the observed variation. In summary, these results suggest that the effect of nitrate on DMS photolysis is important, but generally smaller than AQY variations related to CDOM abundance and quality.[22]

3.4. AQY and Temperature. Toole et al.[24] showed that in Sargasso Sea water AQY followed Arrhenius behavior with an activation energy of ca. 23 kJ mol^{-1}, corresponding to a doubling in AQY (at 320 nm) for every 20 °C increase in temperature. However, this dependence was much weaker (activation energy of ca. 7 kJ mol^{-1}) in Ross Sea Antarctica samples (Westby and Kieber, pers. comm.). Given this large difference in temperature dependence, we reported AQYs at the in situ temperature and did not apply any temperature-dependent correction.

The AQY(330) in samples influenced by the Mississippi River outflow were consistently higher, by 1.8–2.2 -fold, than in samples from the Mackenzie outflow for a given $a_{CDOM}(330)$ (Figure 2B). Since the Mississippi-influenced samples were incubated at a temperature 25 °C higher than Mackenzie-influenced samples, it appears that this 2-fold difference in AQY(330) could be partly or completely accounted for by Arrhenius temperature dependence.

In open-ocean and coastal samples with no riverine influence, AQY(330) was negatively correlated to the sea-surface temperature (SST) in situ ($r_S = -0.45$, $p < 10^{-7}$, $n = 115$) and to the incubation temperature ($r_S = -0.42$, $p < 10^{-6}$). Moreover, SST explained 34% of the linear-space residuals of the regression between AQY(330) and $a_{CDOM}(330)$ (SI Figure S4B). The negative SST dependence of AQY(330), however, does not conform with the Arrhenius behavior previously described. This indicates that SST statistically accounts for other oceanographic factors that control AQY which covary with SST (see section 3.5).

3.5. Multivariate Models. In the previous sections we examined the effect of CDOM, nitrate and temperature on the AQY for DMS photolysis. These variables can be used to improve the statistical prediction of AQY(330), irrespective of the underlying mechanisms. To this end, we performed a stepwise multiple linear regression including $\log_{10}a_{CDOM}(330)$, $\log_{10}NO_3^-$ and SST as initial predictor variables. The p-value for adding a new term was set at 0.01, and that for removing a term at 0.05, and interaction terms were allowed. With these conditions, only CDOM and nitrate remained after the stepwise variable selection, according to the equation:

$$\log_{10} \mathrm{AQY}(330) = (-0.46 \pm 0.04) - (0.84 \pm 0.06) \log_{10} a_{CDOM}(330) + (0.029 \pm 0.003) \log_{10} NO_3^- \quad (9)$$

DOI: 10.1021/acs.est.6b04278
Environ. Sci. Technol. XXXX, XXX, XXX–XXX

with adjusted $r^2 = 0.83$. Thus, nitrate explained 13% additional $\log_{10}$AQY(330) variance compared to the regression model with $a_{CDOM}(330)$ as the only predictor (eq 8). Yet, if nitrate was excluded from the initial set of predictors, a similar amount of variance was explained by including SST in the regression equation:

$$\log_{10} \mathrm{AQY}(330) = (-0.46 \pm 0.07) - (1.58 \pm 0.09) \log_{10} a_{CDOM}(330) + (0.0049 \pm 0.0041)\mathrm{SST} + (0.037 \pm 0.005)\log_{10} a_{CDOM}(330) \times \mathrm{SST} \quad (10)$$

with adjusted $r^2 = 0.82$. This indicates that nitrate and SST are redundant statistical predictors in our data set, which is confirmed by the strong correlation between $\log_{10}NO_3^-$ and SST ($r = -0.63$, $p < 10^{-16}$). In eq 10, the sign of the SST effect on AQY(330) switched from positive to negative for $a_{CDOM}(330)$ less than 0.74 m^{-1}, due to the $a_{CDOM}(330) \times$ SST interaction term. This reflects the occurrence of the highest AQY(330) in cold, CDOM-poor and nitrate-rich sub-Antarctic waters. Alternative regression models including bottom depth and salinity could explain up to 88% of $\log_{10}$AQY(330) variance (not shown), but the large number of regression coefficients (up to 12) rendered them more difficult to interpret and increased the risk of overfitting.[54]

3.6. Conceptual and Modeling Framework. Evidence presented here suggests that CDOM concentration and quality plays a major role in controlling AQY (Figure 2B and 3A–C), with secondary but significant roles for nitrate and temperature. Nevertheless, the importance of different environmental processes varies from coastal to oceanic regions (see graphical abstract).

In coastal areas with sharp a_{CDOM} gradients, progressive dilution and removal of terrestrial CDOM through photodegradation and other processes[27] controls variations in DMS photolysis AQY and k_p. Previous studies have shown that CDOM photobleaching does not affect all chromophores equally, with a preferential removal of condensed aromatic compounds of terrestrial origin compared to aliphatic and carbohydrate-like compounds.[20] Preferential removal of terrestrial chromophores not involved in DMS photolysis would increase the relative amount of DMS photosensitizers offshore, and thus AQY. An alternative and compatible interpretation is possible, by which terrestrial CDOM photobleaching preferentially removes chromophores that quench DMS oxidizers.[26] Irrespective of the mechanism, and although AQY is not methodologically independent from a_{CDOM} (eq 2), their strong negative covariation can be used to model DMS photolysis across sharp estuarine CDOM gradients (eq 8).

Environmental control of AQY(330) in oceanic waters appears more complex than in coastal waters. Our observations support the notion that CDOM composition (or "quality"), rather than CDOM abundance or nitrate concentration (see section 3.3), controls oceanic AQY for DMS photolysis, as proposed by Toole et al.[22] Since CDOM in oceanic waters originates mainly from autochthonous microbial plankton activity,[27] we hypothesize that marine CDOM cycling processes control the AQY for DMS photolysis. If our hypothesis is correct, then spatiotemporal variations in AQY in surface waters should reflect the balance between processes that replenish the upper ocean layer with nonbleached CDOM, such as deep-water upwelling, vertical mixing and phytoplankton blooms,[27,29] and CDOM photodegradation.

Seasonal AQY(330) variations in the Ross Sea (Antarctica) and the NW Mediterranean support this hypothesis (SI Figure S5). In these contrasting locations, AQY(330) decreased by three to 5-fold through spring and summer, whereas concurrent $a_{CDOM}(330)$ variations were less than 2-fold. In the coastal Mediterranean,[38] AQY(330) was negatively correlated to the day of year ($r = -0.93$, $p = 0.0003$), and changed concomitantly with the abundance of various CDOM chromophores of different photolability.[55] Notably, marine CDOM photodegradation in summer is associated with a decrease in the AQY for DMS photolysis, contrary to what is observed for terrestrial CDOM photodegradation. In future studies, advanced chemical characterization of specific chromophores[56,57] could help clarify the findings derived from examination of a_{CDOM} spectral features.

The interplay between ocean circulation and CDOM light history is also illustrated by the high photosensitizer activity associated with upwelled water masses (SI Figure S2), where CDOM may have undergone long-term microbial transformations and relatively little photobleaching.[53,58] Consistent with this interpretation, a few studies have shown[24,26] or suggested[48] that AQY increase with depth in the water column. This issue deserves further attention in future studies, since it might affect the cycling of other climate-relevant trace gases and in regions other than the Southern Ocean.

Our results can be used to better assess DMS photolysis at large-scales, and to understand its response to natural oscillations and global change-driven trends in river discharge,[59] ice cover, vertical mixing, upwelling, and temperature,[60] and potential subsequent changes in nitrate concentration, CDOM absorption and UV penetration.[27] Current biogeochemical models typically represent DMS photolysis as a fixed linear function of irradiance,[61,62] and do not take into account variability in AQY, CDOM, or nitrate. One approach would be to use coupled biogeochemical ocean circulation models to trace the processes responsible for AQY variations. The end-member-like structure that emerges in Figure 3A–C suggests that AQY could be modeled as a function of water mass origin, irradiance exposure at the sea surface and biological cycling of CDOM photosensitizers (distinguishing at least between terrestrial and marine CDOM) and nitrate. Another possibility would be to use empirical parametrizations to statistically predict AQY (eqs 8–10). These parametrizations could be implemented at regional or global scales using remotely sensed CDOM absorption[27] and UV attenuation coefficients in the water column,[63] as well as satellite SST (eq 10) or nitrate derived from climatologies or biogeochemical models (eq 9). Further work is warranted to develop remote sensing models for DMS photolysis.

■ ASSOCIATED CONTENT

Supporting Information

The Supporting Information is available free of charge on the ACS Publications website at DOI: 10.1021/acs.est.6b04278.

The SI includes methodological details for radiative transfer calculations, irradiance units conversion procedures, the nonlinear optimization procedure and the assessment of the effect of nitrate on AQY. Three supporting tables are provided with ancillary data and

DOI: 10.1021/acs.est.6b04278
Environ. Sci. Technol. XXXX, XXX, XXX–XXX

methodological details of individual studies. Five supporting figures are included to further illustrate the relationship between AQY spectra and environmental variables (CDOM, salinity, nitrate and SST) analyzed in the main text. Data are available on request (PDF)

AUTHOR INFORMATION

Corresponding Author

*Phone: 418-656-2131 ×7740; fax: 418-656-2339; e-mail: marti.gali-tapias@takuvik.ulaval.ca.

ORCID

Martí Galí: 0000-0002-5587-1271

David J. Kieber: 0000-0001-6532-950X

Notes

The authors declare no competing financial interest.

ACKNOWLEDGMENTS

We thank the NASA Ocean Biology Distributed Active Archive Center (OB.DAAC) for access to SeaWiFS datasets, Maxime Benoît-Gagné for assistance with radiative transfer computations, and three anonymous reviewers for their constructive comments that helped improve the manuscript. Funding was provided by the (former) Spanish Ministry of Science and Innovation through projects ATOS (POL2006-00550/CTM), SUMMER (CTM2008-03309/MAR) and Malaspina (CSD2008-00077) to RS, and through the National Science Foundation to DJK (ANT-0944686, OCE-0961831). MG acknowledges the receipt of a Beatriu de Pinós postdoctoral fellowship funded by the Generalitat de Catalunya. This is a contribution of the CERC in Remote Sensing of Canada's New Arctic Frontier and Takuvik Joint International Laboratory.

REFERENCES

(1) Simó, R. Production of atmospheric sulfur by oceanic plankton: biogeochemical, ecological and evolutionary links. *Trends Ecol. Evol.* **2001**, *16* (6), 287−294.

(2) Curson, A. R. J.; Todd, J. D.; Sullivan, M. J.; Johnston, A. W. B. Catabolism of dimethylsulphoniopropionate: microorganisms, enzymes and genes. *Nat. Rev. Microbiol.* **2011**, *9* (12), 849−859.

(3) Dickschat, J. S.; Rabe, P.; Citron, C. A. The chemical biology of dimethylsulfoniopropionate. *Org. Biomol. Chem.* **2015**, *13* (7), 1954−1968.

(4) Lana, A.; Bell, T. G.; Simó, R.; Vallina, S. M.; Ballabrera-Poy, J.; Kettle, A. J.; Dachs, J.; Bopp, L.; Saltzman, E. S.; Stefels, J.; et al. An updated climatology of surface dimethlysulfide concentrations and emission fluxes in the global ocean. *Global Biogeochem. Cycles* **2011**, *25*, GB1004.

(5) Land, P. E.; Shutler, J. D.; Bell, T. G.; Yang, M. Exploiting satellite Earth observation to quantify current global oceanic DMS flux and its future climate sensitivity. *J. Geophys. Res. Oceans* **2014**, *119* (11), 7725−7740.

(6) Simó, R. The role of marine microbiota in short-term climate regulation. In *The Role of Marine Biota in the Functioning of the Biosphere*; Duarte, C. M., Ed.; Fundación BBVA, 2011; pp 107−130.

(7) Carpenter, L. J.; Archer, S. D.; Beale, R. Ocean-atmosphere trace gas exchange. *Chem. Soc. Rev.* **2012**, *41*, 6473−6505.

(8) Charlson, R. J.; Lovelock, J. E.; Andreae, M. O.; Warren, S. G. Oceanic phytoplankton, atmospheric sulphur, cloud albedo and climate. *Nature* **1987**, *326*, 655−661.

(9) Lana, A.; Simó, R.; Vallina, S. M.; Dachs, J. Potential for a biogenic influence on cloud microphysics over the ocean: A correlation study with satellite-derived data. *Atmos. Chem. Phys.* **2012**, *12* (17), 7977−7993.

(10) McCoy, D. T.; Burrows, S. M.; Wood, R.; Grosvenor, D. P.; Elliott, S. M.; Ma, P.; Rasch, P. J.; Hartmann, D. L. Natural aerosols explain seasonal and spatial patterns of Southern Ocean cloud albedo. *Sci. Adv.* **2015**, *1*, e1500157.

(11) Nevitt, G. A. The Neuroecology of Dimethyl Sulfide: A Global-Climate Regulator Turned Marine Infochemical. *Integr. Comp. Biol.* **2011**, *51* (5), 819−825.

(12) Amo, L.; Rodríguez-Gironés, M. Á.; Barbosa, A. Olfactory detection of dimethyl sulphide in a krill-eating Antarctic penguin. *Mar. Ecol.: Prog. Ser.* **2013**, *474*, 277−285.

(13) Galí, M.; Simó, R. A meta-analysis of oceanic DMS and DMSP cycling processes: Disentangling the summer paradox. *Global Biogeochem. Cycles* **2015**, *29*, 496−515.

(14) Kiene, R. P.; Bates, T. S. Biological removal of dimethyl sulphide from sea water. *Nature* **1990**, *345*, 702−705.

(15) Brimblecombe, P.; Shooter, D. Photo-oxidation of dimethylsulphide in aqueous solution. *Mar. Chem.* **1986**, *19*, 343−353.

(16) Kieber, D. J.; Jiao, J.; Kiene, R. P.; Bates, T. S. Impact of dimethylsulfide photochemistry on methyl sulfur cycling in the equatorial Pacific Ocean. *J. Geophys. Res.* **1996**, *101* (C2), 3715−3722.

(17) Simó, R.; Pedrós-Alió, C. Short-term variability in the open ocean cycle of dimethylsulfide. *Global Biogeochem. Cycles* **1999**, *13* (4), 1173−1181.

(18) Toole, D. A.; Slezak, D.; Kiene, R. P.; Kieber, D. J.; Siegel, D. A. Effects of solar radiation on dimethylsulfide cycling in the western Atlantic Ocean. *Deep Sea Res., Part I* **2006**, *53*, 136−153.

(19) Galí, M.; Simó, R. Occurrence and cycling of dimethylated sulfur compounds in the Arctic during summer receding of the ice edge. *Mar. Chem.* **2010**, *122*, 105−117.

(20) Mopper, K.; Kieber, D. J.; Stubbins, A. Marine Photochemistry of Organic Matter: Processes and Impacts. In *Biogeochemistry of Marine Dissolved Organic Matter*; Hansell, D. A., Carlson, C. A., Eds.; Academic Press, 2015; pp 389−450.

(21) Bouillon, R.-C.; Miller, W. L. Determination of apparent quantum yield spectra of DMS photo-degradation in an in situ iron-induced Northeast Pacific Ocean bloom. *Geophys. Res. Lett.* **2004**, *31* (6), L06310.

(22) Toole, D. A.; Kieber, D. J.; Kiene, R. P.; White, E. M.; Bisgrove, J.; del Valle, D. A.; Slezak, D. High dimethylsulfide photolysis rates in nitrate-rich Antarctic waters. *Geophys. Res. Lett.* **2004**, *31* (11), L11307.

(23) Bouillon, R.-C.; Miller, W. L. Photodegradation of dimethyl sulfide (DMS) in natural waters: laboratory assessment of the nitrate-photolysis-induced DMS oxidation. *Environ. Sci. Technol.* **2005**, *39* (24), 9471−9477.

(24) Toole, D. A.; Kieber, D. J.; Kiene, R. P.; Siegel, D. A.; Nelson, N. B. Photolysis and the dimethylsulfide (DMS) summer paradox in the Sargasso Sea. *Limnol. Oceanogr.* **2003**, *48* (3), 1088−1100.

(25) Deal, C.; Kieber, D. J.; Toole, D. A.; Stamnes, K.; Jiang, S.; Uzuka, N. Dimethylsulfide photolysis rates and apparent quantum yields in Bering Sea seawater. *Cont. Shelf Res.* **2005**, *25* (15), 1825−1835.

(26) Taalba, A.; Xie, H.; Scarratt, M. G.; Bélanger, S.; Levasseur, M. Photooxidation of dimethylsulfide (DMS) in the Canadian Arctic. *Biogeosciences* **2013**, *10* (11), 6793−6806.

(27) Nelson, N. B.; Siegel, D. A. The global distribution and dynamics of chromophoric dissolved organic matter. *Annu. Rev. Mar. Sci.* **2013**, *5*, 447−476.

(28) Nelson, N. Production of chromophoric dissolved organic matter by Sargasso Sea microbes. *Mar. Chem.* **2004**, *89* (1), 273−287.

(29) Romera-Castillo, C.; Sarmento, H.; Álvarez-Salgado, X. A.; Gasol, J. M.; Marrasé, C. Production of chromophoric dissolved organic matter by marine phytoplankton. *Limnol. Oceanogr.* **2010**, *55* (1), 446−454.

(30) Bélanger, S.; Xie, H.; Krotkov, N.; Larouche, P.; Vincent, W. F.; Babin, M. Photomineralization of terrigenous dissolved organic matter in Arctic coastal waters from 1979 to 2003: Interannual variability and implications of climate change. *Global Biogeochem. Cycles* **2006**, *20* (4), GB4005.

DOI: 10.1021/acs.est.6b04278
Environ. Sci. Technol. XXXX, XXX, XXX−XXX

(31) Fichot, C. G.; Miller, W. L. An approach to quantify depth-resolved marine photochemical fluxes using remote sensing: Application to carbon monoxide (CO) photoproduction. *Remote Sens. Environ.* **2010**, *114* (7), 1363−1377.
(32) Locarnini, R. A.; Mishonov, A. V.; Antonov, J. I.; Boyer, T. P.; Garcia, H. E.; Baranova, O. K.; Zweng, M. M.; Paver, C. R.; Reagan, J. R.; Johnson, D. R.; et al. *World Ocean Atlas 2013, Volume 1: Temperature*. Levitus, S., Mishonov, A., Eds.; Technical Ed.; NOAA Atlas NESDIS 73, 2013; 40 pp.
(33) Zweng, M. M.; Reagan, J. R.; Antonov, J. I.; Mishonov, A. V.; Boyer, T. P.; Garcia, H. E.; Baranova, O. K.; Johnson, D. R.; Seidov, D.; Biddle, M. M. *World Ocean Atlas 2013, Volume 2: Salinity*. Levitus, S., Mishonov, A., Eds.; Technical Ed.; NOAA Atlas NESDIS 74, 2013; 39 pp.
(34) Garcia, H. E.; Locarnini, R. A.; Boyer, T. P.; Antonov, J. I.; Baranova, O. K.; Zweng, M. M.; Reagan, J. R.; D.R, J. *World Ocean Atlas 2013, Vol. 4: Dissolved Inorganic Nutrients (phosphate, nitrate, silicate)*. Levitus, S., Mishonov, A., Eds.; Technical Ed.; NOAA Atlas NESDIS 76, 2013.
(35) Helms, J. R.; Stubbins, A.; Ritchie, J. D.; Minor, E. C.; Kieber, D. J.; Mopper, K. Absorption spectral slopes and slope ratios as indicators of molecular weight, source, and photobleaching of chromophoric dissolved organic matter. *Limnol. Oceanogr.* **2008**, *53* (3), 955−969.
(36) Dahlén, J.; Bertilsson, S.; Pettersson, C. Effects of UV-A irradiation on dissolved organic matter in humic surface waters. *Environ. Int.* **1996**, *22* (5), 501−506.
(37) Weishaar, J. L.; Aiken, G. R.; Bergamaschi, B. A.; Fram, M. S.; Fujii, R.; Mopper, K. Evaluation of Specific Ultraviolet Absorbance as an Indicator of the Chemical Composition and Reactivity of Dissolved Organic Carbon. *Environ. Sci. Technol.* **2003**, *37* (20), 4702−4708.
(38) Galí, M.; Ruiz-González, C.; Lefort, T.; Gasol, J. M.; Cardelús, C.; Romera-Castillo, C.; Simó, R. Spectral irradiance dependence of sunlight effects on plankton dimethylsulfide production. *Limnol. Oceanogr.* **2013**, *58* (2), 489−504.
(39) R Core Team. *R: A Language and Environment for Statistical Computing*; R Foundation for Statistical Computing: Vienna, Austria, 2015. ISBN 3-900051-07-0, URL http://www.R-project.org/.
(40) Graves, S.; Piepho, H.-P.; Selzer, L.; Dorai-Raj, S. multcompView: Visualizations of Paired Comparisons. R package version 0.1−7. URL http://cran.r-project.org/package=multcompView. 2015.
(41) Ricchiazzi, P.; Yang, S.; Gautier, C.; Sowle, D. SBDART: A Research and Teaching Software Tool for Plane-Parallel Radiative Transfer in the Earth's Atmosphere. *Bull. Am. Meteorol. Soc.* **1998**, *79* (10), 2101−2114.
(42) Bélanger, S.; Babin, M.; Tremblay, J.-E. Increasing cloudiness in Arctic damps the increase in phytoplankton primary production due to sea ice receding. *Biogeosciences* **2013**, *10*, 4087−4101.
(43) Kieber, D. J.; Miller, G. W.; Neale, P. J.; Mopper, K. Wavelength and temperature-dependent apparent quantum yields for photochemical formation of hydrogen peroxide in seawater. *Environ. Sci. Process. Impacts* **2014**, *16* (4), 777−791.
(44) Bailey, K. E.; Toole, D. A.; Blomquist, B.; Najjar, R. G.; Huebert, B.; Kieber, D. J.; Kiene, R. P.; Matrai, P.; Westby, G. R.; del Valle, D. A. Dimethylsulfide production in Sargasso Sea eddies. *Deep Sea Res., Part II* **2008**, *55*, 1491−1504.
(45) Galí, M.; Saló, V.; Almeda, R.; Calbet, A.; Simó, R. Stimulation of gross dimethylsulfide (DMS) production by solar radiation. *Geophys. Res. Lett.* **2011**, *38* (15), GL048051.
(46) Galí, M.; Simó, R.; Pérez, G. L.; Ruiz-González, C.; Sarmento, H.; Fuentes-Lema, A.; Royer, S.-J.; Gasol, J. M. Differential response of planktonic primary, bacterial, and dimethylsulfide production rates to vertically-moving and static incubations in upper mixed-layer summer sea waters. *Biogeosciences* **2013**, *10*, 7983−7998.
(47) Hatton, A. D. Influence of photochemistry on the marine biogeochemical cycle of dimethylsulphide in the northern North Sea. *Deep Sea Res., Part II* **2002**, *49*, 3039−3052.
(48) Belviso, S.; Bopp, L.; Mosseri, J.; Tedetti, M.; Garcia, N.; Griffiths, B.; Joux, F.; Obernosterer, I.; Uitz, J.; Veldhuis, M. Effect of natural iron fertilisation on the distribution of DMS and DMSP in the Indian sector of the Southern Ocean. *Deep Sea Res., Part II* **2008**, *55* (5−7), 893−900.
(49) Orsi, A. H.; Whitworth, T.; Nowlin, W. D. On the meridional extent and fronts of the Antarctic Circumpolar Current. *Deep Sea Res., Part I* **1995**, *42* (5), 641−673.
(50) England, M. H. The age of water and ventilation timescales in a global ocean model. *J. Phys. Oceanogr.* **1995**, *25*, 2756−2777.
(51) Brugger, A.; Slezak, D.; Obernosterer, I.; Herndl, G. J. Photolysis of dimethylsulfide in the northern Adriatic Sea: Dependence on substrate concentration, irradiance and DOC concentration. *Mar. Chem.* **1998**, *59*, 321−331.
(52) Herrmann, M.; Najjar, R. G.; Neeley, A. R.; Vila-Costa, M.; Dacey, J. W. H.; DiTullio, G. R.; Kieber, D. J.; Kiene, R. P.; Matrai, P. A.; Simó, R.; et al. Diagnostic modeling of dimethylsulfide production in coastal water west of the Antarctic Peninsula. *Cont. Shelf Res.* **2012**, *32*, 96−109.
(53) Catalá, T. S.; Reche, I.; Álvarez, M.; Khatiwala, S.; Guallart, E. F.; Benítez-Barrios, V. M.; Fuentes-Lema, A.; Romera-Castillo, C.; Nieto-Cid, M.; Pelejero, C.; et al. Water Mass Age and Ageing Driving Chromophoric Dissolved Organic Matter in the Dark Global Ocean. *Global Biogeochem. Cycles* **2015**, *29*, GB005048.
(54) Hawkins, D. M. The Problem of Overfitting. *J. Chem. Inf. Comput. Sci.* **2004**, *44*, 1−12.
(55) Romera-Castillo, C.; Álvarez-Salgado, X. A.; Galí, M.; Gasol, J. M.; Marrasé, C. Combined effect of light exposure and microbial activity on distinct dissolved organic matter pools. A seasonal field study in an oligotrophic coastal system (Blanes Bay, NW Mediterranean). *Mar. Chem.* **2013**, *148*, 44−51.
(56) Stubbins, A.; Lapierre, J. F.; Berggren, M.; Prairie, Y. T.; Dittmar, T.; Del Giorgio, P. A. What's in an EEM? Molecular signatures associated with dissolved organic fluorescence in boreal Canada. *Environ. Sci. Technol.* **2014**, *48* (18), 10598−10606.
(57) Repeta, D. J. Chemical Characterization and Cycling of Dissolved Organic Matter. In *Biogeochemistry of Marine Dissolved Organic Matter*; Hansell, D. A., Carlson, C. A., Eds.; Academic Press, 2015; pp 21−63.
(58) De la Fuente, P.; Marrasé, C.; Canepa, A.; Álvarez-salgado, X. A.; Gasser, M.; Fajar, N. M.; Romera-Castillo, C.; Pelegrí, J. L. Does a general relationship exist between fluorescent dissolved organic matter and microbial respiration? — The case of the dark equatorial Atlantic Ocean. *Deep Sea Res., Part I* **2014**, *89*, 44−55.
(59) Milliman, J. D.; Farnsworth, K. L.; Jones, P. D.; Xu, K. H.; Smith, L. C. Climatic and anthropogenic factors affecting river discharge to the global ocean, 1951−2000. *Glob. Planet. Change* **2008**, *62*, 187−194.
(60) Stocker, T. F.; Qin, D.; Plattner, G.-K.; Alexander, L. V.; Allen, S. K.; Bindoff, N. L.; Bréon, F.-M.; Church, J. A.; Cubasch, U.; Emori, S.; et al. Technical Summary. In *Climate Change 2013: The Physical Science Basis. Contribution of Working Group I to the Fifth Assessment Report of the Intergovernmental Panel on Climate Change*; Stocker, T. F., Qin, D., Plattner, G.-K., Tignor, M., Allen, S. K., Boschung, J., Nauels, A., Xia, Y., Bex, V., Midgley, P. M., Eds.; Cambridge University Press: Cambridge, United Kingdom and New York, NY, USA., 2013; pp 33−115.
(61) Bopp, L.; Aumont, O.; Belviso, S.; Blain, S. Modelling the effect of iron fertilization on dimethylsulphide emissions in the Southern Ocean. *Deep Sea Res., Part II* **2008**, *55*, 901−912.
(62) Vogt, M.; Vallina, S. M.; Buitenhuis, E. T.; Bopp, L.; Le Quéré, C. Simulating dimethylsulphide seasonality with the Dynamic Green Ocean Model PlankTOM5. *J. Geophys. Res.* **2010**, *115*, C06021.
(63) Cao, F.; Fichot, C. G.; Hooker, S. B.; Miller, W. L. Improved algorithms for accurate retrieval of UV/visible diffuse attenuation coefficients in optically complex, inshore waters. *Remote Sens. Environ.* **2014**, *144*, 11−27.

DOI: 10.1021/acs.est.6b04278
Environ. Sci. Technol. XXXX, XXX, XXX−XXX